Collective Lamb Shift in Single-Photon Superradiance

Ralf Röhlsberger, *et al.*

Science **328**, 1248 (2010);
DOI: 10.1126/science.1187770

that the excitations are mobile to a distance 1000 times as long as the interspin distance without being scattered. Remarkably, the observed ℓ_s is even longer than the mean impurity distance estimated from the susceptibility measurements (*5*). Although our simple estimation should be scrutinized, the nearly ballistic propagation seems to be realized in this QSL state, which bears a striking resemblance to the 1D Heisenberg system (*25*). Such a coherent motion of the excitation is only possible with an extremely long correlation length, consistent with the power-law correlation function with gapless excitations.

Our results indicate that there are two kinds of excitations in the low-temperature regime of dmit-131: One is a low-lying gapless excitation and another is a spin-gap–like excitation that couples to magnetic fields. The existence of the gapless mode imposes constraints on theories that can account for the QSL in this material. For instance, it contradicts the identification of the ground state of this system with a fully gapped short-range resonating-valence-bond state (*27*). It is intriguing that, although there has been no experimental observation, the coexistence of the gapless and gapped excitations has been theoretically predicted in highly frustrated kagomé lattice (*28*). In this case, the magnetic excitations are separated from the ground state by a spin-gap, which is filled with nonmagnetic excitations. It is a nontrivial problem, however, if such a state can be realized in a triangular lattice where less quantum degenerate states are expected.

Recently, the ground state of a QSL in the 2D triangular lattice has been discussed in terms of the spinon Fermi surface (*7*, *8*). The Fermi surface is suggested to have pairing instability at low temperatures, and a possible nodal gap structure appears that is analogous to *d*-wave superconductivity in high-transition temperature cuprates (*29*). In this scenario, the spin-gap–like behavior is attributed to the pairing gap formation, and the finite residual *T*-linear term stems from the zero-energy density of states similar to the disorder-induced normal fluid in *d*-wave superconductors. The low energy density of states is expected to be insensitive to Zeeman magnetic field as in a Fermi liquid. The nodal gap is expected to produce thermally excited quasiparticles, which may account for the observed T^2 dependence of κ/T with a much steeper slope than κ_{xx}^{ph}/T (Fig. 2C). This model also predicts a thermal-Hall effect of spinons that experience the Lorentz force, akin to the conduction electrons in metals (*30*). In an attempt to observe this effect, we measured the thermal-Hall conductivity κ_{xy}, and the tangent of the thermal-Hall angle, $\tan\theta(H) = \kappa_{xy}/(\kappa_{xx} - \kappa_{xx}^{ph})$ (Fig. 3B). The observed thermal-Hall angle is orders of magnitude smaller than the prediction (*26*), which calls for further studies. It is also an open question why continuous excitations are observed in the present compound whereas they are absent in κ-$(BEDT\text{-}TTF)_2Cu_2(CN)_3$ (*18*). Such excitations may be strongly suppressed by inhomogeneity.

References and Notes

1. P. A. Lee, *Science* **321**, 1306 (2008).
2. P. W. Anderson, *Science* **235**, 1196 (1987).
3. Y. Shimizu, K. Miyagawa, K. Kanoda, M. Maesato, G. Saito, *Phys. Rev. Lett.* **91**, 107001 (2003).
4. T. Itou, A. Oyamada, S. Maegawa, M. Tamura, R. Kato, *J. Phys. Conf. Ser.* **145**, 012039 (2009).
5. T. Itou, A. Oyamada, S. Maegawa, M. Tamura, R. Kato, *Phys. Rev. B* **77**, 104413 (2008).
6. D. A. Huse, V. Elser V, *Phys. Rev. Lett.* **60**, 2531 (1988).
7. O. I. Motrunich, *Phys. Rev. B* **72**, 045105 (2005).
8. S.-S. Lee, P. A. Lee, *Phys. Rev. Lett.* **95**, 036403 (2005).
9. X.-G. Wen, *Phys. Rev. B* **65**, 165113 (2002).
10. D. N. Sheng, O. I. Motrunich, M. P. A. Fisher, *Phys. Rev. B* **79**, 205112 (2009).
11. G. Misguich, C. Lhuillier, B. Bernu, C. Waldtmann, *Phys. Rev. B* **60**, 1064 (1999).
12. Y. Qi, C. Xu, S. Sachdev, *Phys. Rev. Lett.* **102**, 176401 (2009).
13. V. Kalmeyer V, R. B. Laughlin, *Phys. Rev. Lett.* **59**, 2095 (1987).
14. H. Morita, S. Watanabe, M. Imada, *J. Phys. Soc. Jpn.* **71**, 2109 (2002).
15. T. Yoshioka, A. Koga, N. Kawakami, *Phys. Rev. Lett.* **103**, 036401 (2009).
16. S. Yunoki, S. Sorella, *Phys. Rev. B* **74**, 014408 (2006).
17. Y. Hayashi, M. Ogata, *J. Phys. Soc. Jpn.* **76**, 053705 (2007).
18. M. Yamashita *et al.*, *Nat. Phys.* **5**, 44 (2009).
19. L. D. Faddeev, L. A. Takhtajan, *Phys. Lett.* **85A**, 375 (1981).
20. F. D. M. Haldane, *Phys. Lett.* **93A**, 464 (1983).
21. S. Yamashita *et al.*, *Nat. Phys.* **4**, 459 (2008).
22. Y. Shimizu, K. Miyagawa, K. Kanoda, M. Maesato, G. Saito, *Phys. Rev. B* **73**, 140407 (2006).
23. R. S. Manna, M. de Souza, A. Brühl, J. A. Schlueter, M. Lang, *Phys. Rev. Lett.* **104**, 016403 (2010).
24. M. Tamura, R. Kato, *Polyhedron* **24**, 2817 (2005).
25. A. V. Sologubenko, K. Giannò, H. R. Ott, A. Vietkine, A. Revcolevschi, *Phys. Rev. B* **64**, 054412 (2001).
26. Materials and methods are available as supporting material on *Science* Online.
27. R. Moessner, S. L. Sondhi, *Phys. Rev. Lett.* **86**, 1881 (2001).
28. Ch. Waldtmann *et al.*, *Eur. Phys. J. B* **2**, 501 (1998).
29. T. Grover, N. Trivedi, T. Senthil, P. A. Lee, "Weak Mott insulators on the triangular lattice: Possibility of a gapless nematic quantum spin liquid;" http://arxiv.org/abs/0907.1710 (2009).
30. H. Katsura, N. Nagaosa, P. A. Lee, *Phys. Rev. Lett.* **104**, 066403 (2010).

31. We thank M. P. A. Fisher, S. Fujimoto, T. Itou, H. Katsura, N. Kawakami, H. Kawamura, P. A. Lee, G. Misguich, Y. Nakazawa, and A. Tanaka for valuable discussion. This work was supported by Grants-in-Aid for Scientific Research (KAKENHI) from the Japan Society for the Promotion of Science and the Ministry of Education, Culture, Sports, Science, and Technology (MEXT), a Grant-in-Aid for the Global Centers of Excellence Program "The Next Generation of Physics, Spun from Universality and Emergence," and a Grant-in-Aid for Scientific Research on Innovative Areas "Heavy Electrons" (No. 20102006) from MEXT, Japan.

Supporting Online Material

www.sciencemag.org/cgi/content/full/328/5983/1246/DC1
Materials and Methods
Figs. S1 and S2
Table S1
References

10 February 2010; accepted 29 April 2010
10.1126/science.1188200

Collective Lamb Shift in Single-Photon Superradiance

Ralf Röhlsberger,[1]* Kai Schlage,[1] Balaram Sahoo,[1] Sebastien Couet,[2] Rudolf Rüffer[3]

Superradiance, the cooperative spontaneous emission of photons from an ensemble of identical atoms, provides valuable insights into the many-body physics of photons and atoms. We show that an ensemble of resonant atoms embedded in the center of a planar cavity can be collectively excited by synchrotron radiation into a purely superradiant state. The collective coupling of the atoms via the radiation field leads to a substantial radiative shift of the transition energy, the collective Lamb shift. We simultaneously measured the temporal evolution of the superradiant decay and the collective Lamb shift of resonant ^{57}Fe nuclei excited with 14.4–kilo–electron volt synchrotron radiation. Our experimental technique provides a simple method for spectroscopic analysis of the superradiant emission.

The development of quantum electrodynamics is very closely related to the discovery and explanation of the Lamb shift of atomic energy levels (*1*, *2*). The Lamb shift is a small energy shift of bound atomic states, mainly resulting from the emission and reabsorption of virtual photons within the same atom. An additional contribution emerges if many identical two-level atoms are interacting collectively with a resonant radiation field. In this case, a virtual photon that is emitted by one atom may be reabsorbed by another atom within the ensemble. The resulting collective Lamb shift scales with the optical density of the atoms and sensitively depends on their spatial arrangement (*3*–*9*). At high atomic densities, however, atom-atom interactions mask the collective Lamb shift, making it almost impossible to observe. Since the early theoretical studies (*3*), only one measurement of a collective line shift has been reported for a multiphoton excitation scheme in a noble gas (*10*, *11*). Experimental assessment of the collective Lamb

[1]Deutsches Elektronen Synchrotron DESY, Notkestr. 85, 22607 Hamburg, Germany. [2]Instituut voor Kern- en Stralingsfysica and INPAC, Katholieke Universiteit Leuven, Celestijnenlaan 200D, B-3001 Leuven, Belgium. [3]European Synchrotron Radiation Facility, B.P. 220, 38043 Grenoble Cedex, France.

*To whom correspondence should be addressed. E-mail: ralf.roehlsberger@desy.de

shift for single-photon excitation, particularly in solid-state samples, has remained elusive. Here, we measured the collective Lamb shift for an ensemble of ^{57}Fe Mössbauer nuclei (transition energy $E_0 = \hbar\omega_0 = 14.4$ keV, level width $\Gamma_0 = 4.7$ neV, natural lifetime $\tau_0 = \hbar/\Gamma_0 = 141$ ns, where ω_0 is the frequency and $\hbar$ is the Planck constant divided by 2π), embedded in a planar cavity that was resonantly excited by synchrotron radiation x-rays.

The collective Lamb shift is a cooperative optical effect that is intimately connected with the phenomenon of superradiance—the cooperative spontaneous emission of radiation from an ensemble of identical two-level atoms, introduced by Dicke in 1954 (*12*) and observed experimentally after short-pulse lasers became available (*13*, *14*). Superradiance was originally conceived by Dicke for sample dimensions R much smaller than the wavelength $\lambda = 2\pi c/\omega_0$ of the resonant transition (where c is the speed of light). In this limit, an ensemble of N atoms, excited by a single photon, decays collectively N times as quickly as a single isolated atom. It is, however, the opposite limit $R >> \lambda$ that is relevant for most experiments in the optical or x-ray regimes. For an extended sample, the state vector of the atomic ensemble is given by

$$|\psi_+\rangle_{k_0} = \frac{1}{\sqrt{N}}\sum_j \exp(i\mathbf{k}_0 \cdot \mathbf{r}_j)|b_1 b_2 \ldots a_j \ldots b_N\rangle \quad (1)$$

where $|b_1\ b_2\ \ldots\ a_j\ \ldots\ b_N\rangle$ is a Fock state in which the jth atom at position $\mathbf{r}_j$ is in the excited state a and all other atoms are in the ground state b. Because the positions $\mathbf{r}_j$ translate to different times of excitation t_j for pulsed directional excitation with wave vector $\mathbf{k}_0$, $t_j = \mathbf{k}_0 \cdot \mathbf{r}_j/\omega_0$, this state has been called the "timed" Dicke state (*15*), closely resembling the "nuclear exciton" state for ensembles of Mössbauer nuclei collectively excited by synchrotron radiation (*16*). The spatial phase factors of the timed Dicke state lead to directional emission along $\mathbf{k}_0$ (*15*, *16*), with the temporal evolution of its probability amplitude given by $\beta_+(t) = \beta_0 \exp[-(1/2)(\Gamma_0 + \Gamma_N + iL_N)t/\hbar]$, where Γ_0 is the single-atom decay width, Γ_N is the N-atom decay width, and L_N is the collective Lamb shift. This shows that the emission from extended samples can exhibit Dicke-like superradiant dynamics as in the limit $R << \lambda$ (*5*, *6*). In this case, the collective Lamb shift is not masked by atom-atom interactions as in the small-sample limit, thus becoming experimentally accessible.

Note that the preparation of the timed Dicke state requires the excitation probability to be uniform over the sample (*17*). In conventional forward scattering, however, the timed Dicke state can never be created exactly because the radiation from atoms at the entrance front of the sample interferes destructively with radiation from atoms deeper in the sample (*16*). The result is a nonuniformly excited ensemble of atoms. With increasing time after excitation, a substantial fraction of nonsuperradiant, slowly decaying states is populated (*16*, *18*). The interference of these states results in temporal oscillations that are often referred to as dynamical beats or propagation quantum beats (*19*). To avoid the population of nonsuperradiant states, it is necessary for the sample to be optically thin upon absorption and optically thick upon emission in order to exhibit strong superradiant enhancement (*20*).

We prepare the timed Dicke state of Eq. 1 by embedding an ensemble of ^{57}Fe atoms in a planar low-Q cavity ($Q < 100$) and resonantly exciting them with synchrotron radiation pulses coupled evanescently into the first-order mode (Fig. 1). The cavity geometry exhibits a number of important features that facilitate the observation of the collective Lamb shift. First, the ensemble appears to be optically thin upon absorption, with the excitation probability for all atoms within the ensemble being practically the same. Second, the partial waves emitted from the ensemble are funneled into a single mode of the cavity, yielding a total amplitude corresponding to the emission from an optically thick sample. Therefore, the optical thicknesses of the sample for absorption and emission are effectively decoupled. Finally, the cavity enhances the photonic density of states at the position of the atoms, which strongly amplifies the radiative level shift, as has been shown for single atoms in cavities (*21*).

In a typical cavity used here (Fig. 1), a material of low electron density (C, 32 nm thick) is sandwiched between two layers of high electron density (Pt). The top Pt layer is thin enough (2.2 nm) that x-rays impinging under grazing angles can evanescently couple into the cavity. Guided modes are excited at angles of incidence where deep minima in the x-ray reflectivity appear (Fig. 1B). An ensemble of ^{57}Fe nuclei is embedded as ultrathin layer within the guiding layer of the cavity. The spectral response of this system (i.e., its reflectivity R in the vicinity of the nuclear resonance) is calculated by introducing the nuclear forward scattering amplitude f_N of the resonant layer material. If we assume that the nuclei within the ensemble exhibit a single Lorentzian resonance line, then f_N is given by

$$f_N(x) = \frac{2\pi c_N \rho_N}{k_0 k_{0z}}\left[\frac{1}{x+i}\right] \quad (2)$$

where $k_{0z} \approx k_0\varphi$ is the component of the wave vector k_0 normal to the surface, ρ_N is the number density of resonant nuclei, c_N combines nuclear parameters (*22*), and $x = \Delta E/(\Gamma_0/2)$ describes the detuning $\Delta E = E - E_0$ of the photon energy from the exact resonance energy E_0. We perform a perturbation expansion of the nuclear resonant reflectivity R of the cavity in powers of f_N. A diagrammatical representation of the perturbation series of R (Fig. 1A) shows that the amplitudes A_i of the partial waves emitted from the nuclear ensemble at the "vertices" (black dots) correspond to the various orders of the perturbation expansion. The scattered amplitude in the nth outgoing wave is related to the $(n-1)$th amplitude via $A_n =$

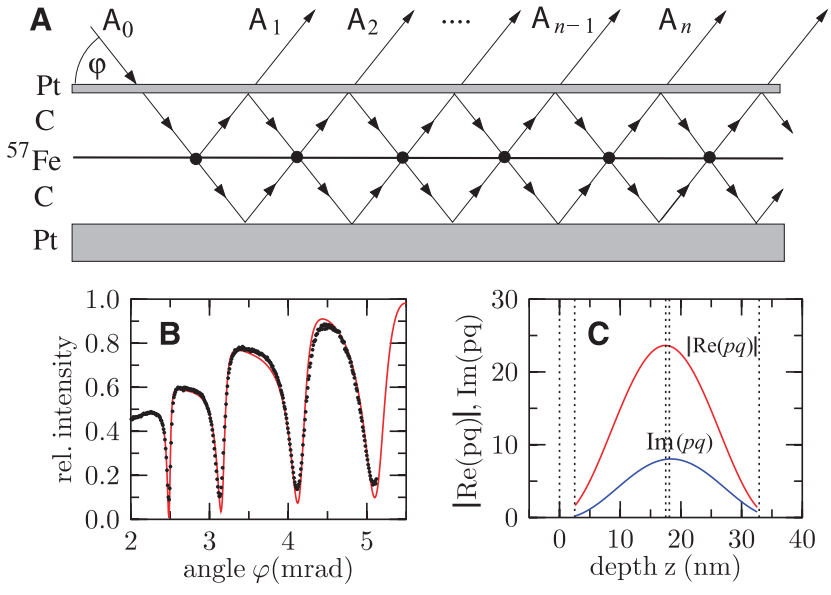

Fig. 1. (**A**) Structure of the planar cavity and scattering geometry used for calculation of the collective Lamb shift for the resonant ^{57}Fe nuclei embedded in the planar cavity. (**B**) Measured (nonresonant) x-ray reflectivity of one of the samples (sample 1) used in the experiment, consisting of (2.2 nm Pt)/(16 nm C)/(0.6 nm ^{57}Fe)/(16 nm C)/(13 nm Pt) deposited on a superpolished Si substrate with a root-mean-square roughness below 0.3 nm. The solid line is a fit to the data, from which the exact values of the layer thicknesses were determined. Guided modes are excited at the angular positions of the minima. (**C**) The quantities Im(pq) and |Re(pq)| as function of depth in the first-order mode (*23*). Dashed lines mark the interfaces between layers.

(idf_N)pqA_{n-1}, where d is the thickness of the ^{57}Fe layer and p and q are the amplitudes of the wave fields (at the position of the resonant nuclei) propagating in the directions of the incident and the reflected beams, respectively. p and q can be calculated via a propagation matrix formalism (*23*). The depth dependence of the relevant product pq for the first-order mode of the cavity used here is shown in Fig. 1C. For the first vertex, we have $A_1 = (idf_N)p^2A_0$, which also includes the coupling of the radiation into the cavity. Thus, the sum over all orders results in

$$R = idf_N p^2 \sum_{k=0}^{\infty} (idpqf_N)^k = \frac{idp^2 f_N}{1 - idpqf_N} \quad (3)$$

Inserting $f_N(x) = C/(x + i)$, where $C = 2\pi c_N \rho_N d/(k_0 k_{0z})$ and $x = \Delta E/(\Gamma_0/2)$, we obtain again a Lorentzian resonance line $R(\Delta E) = Cp^2(\Gamma_0/2)/[\Delta E + L_N + i(\Gamma_0 + \Gamma_N)/2]$ that exhibits a collective decay width of $\Gamma_N = C|\mathrm{Re}(pq)|\Gamma_0 = \chi\Gamma_0$ (where χ is the collective enhancement factor) and an energy shift of $L_N = -C[\mathrm{Im}(pq)\Gamma_0/2]$. Because the factor C scales with the density ρ_N of the resonant nuclei, the energy shift is essentially the collective Lamb shift of the ensemble of nuclei in the cavity. Explicitly, the collective Lamb shift is given by

$$L_N = -\frac{1}{2}\left[\frac{2\pi c_N \rho_N}{k_0^2}\frac{d}{\varphi}\Gamma_0\right]\mathrm{Im}(pq) \quad (4)$$

The expression in square brackets is the collective decay width for the free-standing layer of resonant nuclei illuminated under an angle φ. The factor Im(pq) describes the enhancement due to the cavity. In the first-order mode, Im(pq) peaks in the center of the guiding layer (Fig. 1C). For a nuclear ensemble placed at that depth, one can expect a radiative level shift up to $-13\Gamma_0$, depending on the layer materials the cavity consists of. This value is eventually limited by the electronic photoabsorption of the Fe atoms, which disturbs the wave field in the cavity.

To observe these effects, we prepared cavity samples containing ultrathin ^{57}Fe layers with thicknesses of 0.6 nm (sample 1) and 1.2 nm (sample 2) by physical vapor deposition techniques (*23*). After pulsed resonant excitation at $t = 0$ with synchrotron radiation (*23*), we observed for both samples an exponential decay $I(t) = I_0 \exp[-(\Gamma_0 + \Gamma_N)t/\hbar] = I_0 \exp[-(1 + \chi)t/\tau_0]$ over two orders of magnitude from $t = 6$ ns until $t = 20$ ns (Fig. 2). χ describes the speedup of the decay with values of $\chi = 42$ and $\chi = 61$ for samples 1 and 2, respectively.

After 20 ns, the temporal response levels off into a much slower decay, caused by inhomogeneous broadening and a residual quadrupole hyperfine interaction of the nuclei in the sample. The inset of Fig. 2 shows a conversion electron Mössbauer (CEMS) spectrum of ^{57}Fe (0.6 nm) embedded in a carbon matrix from which a quadrupole splitting (QS) of 33.8 neV, an isomer shift of 4.7 neV, and a QS distribution of 37.6 neV (full width at half maximum) was derived. Taking into account the measured hyperfine interaction parameters, we used the dynamical theory of nuclear resonant scattering (*16*, *24*–*26*) to calculate the temporal evolution of the nuclear decay and obtained very good agreement with the measured data. As the width of the inhomogeneously broadened resonance line is much smaller than the collective decay width Γ_N, the inhomogeneous dephasing has negligible effects on the superradiant decay (*23*, *27*, *28*). Thus, the observation of the initial,

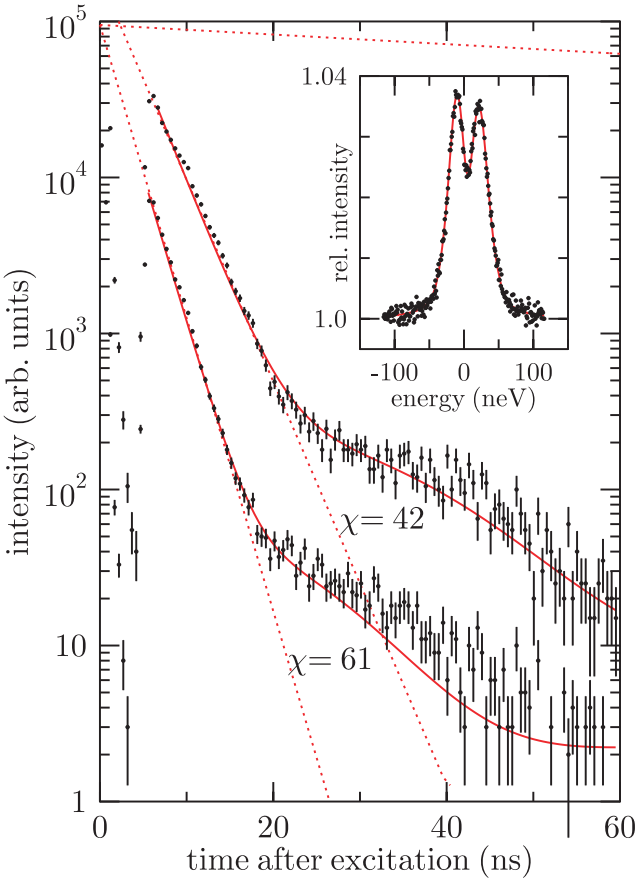

Fig. 2. Nuclear resonant time response of the two samples upon excitation of the first-order guided mode in sample 1 (0.6 nm ^{57}Fe, upper curve) and sample 2 (1.2 nm ^{57}Fe, lower curve). Both curves are displaced along the ordinate for better visualization. The solid lines are theoretical calculations taking into account the hyperfine interaction of the ^{57}Fe nuclei as derived from the CEMS spectrum shown in the inset. From the initial slope of both curves, speedup values of $\chi = 42$ and $\chi = 61$, respectively, are determined. The dotted line at the top of the figure displays the natural decay of the ^{57}Fe.

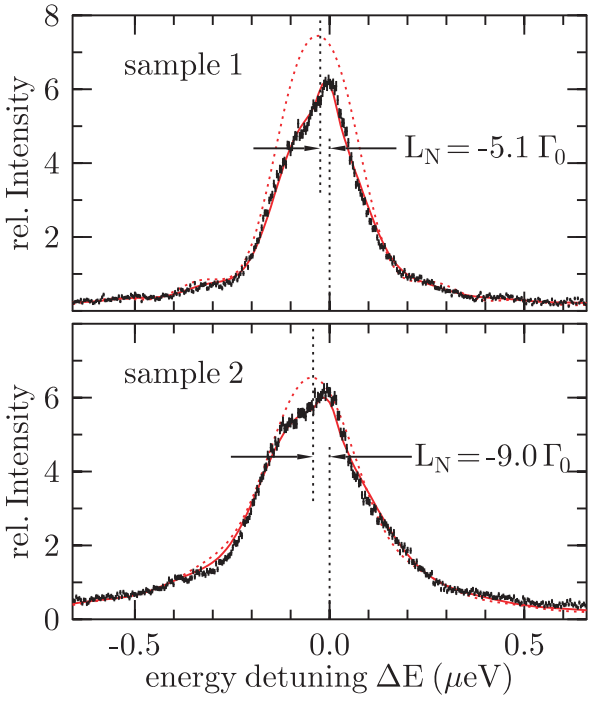

Fig. 3. Energy response of the two samples, as recorded using a stainless steel foil (thickness 5.6 μm) as an analyzer. Delayed quanta were collected in a time window between 22 ns and 160 ns. The shift of the center of mass of these curves relative to the origin corresponds to the collective Lamb shift. The collective decay widths are $\Gamma_N = 45\Gamma_0$ and $\Gamma_N = 65\Gamma_0$, respectively. Solid red curves are theoretical calculations according to (*23*). For comparison, the dashed red lines are calculations assuming vanishing hyperfine interaction.

strictly exponential decay in Fig. 2 proves the formation of the timed Dicke state in Eq. 1 and its superradiant decay.

According to Eq. 4, we expect a collective Lamb shift of several natural linewidths Γ_0 for both samples. To measure this shift, we analyzed the energy spectra $|R(E)|^2$ of the radiation reflected from the samples. For that purpose, we used a Doppler drive (as used in conventional Mössbauer spectroscopy) on which a thin foil (thickness 5.6 μm) consisting of stainless steel with the composition $^{57}Fe_{55}Cr_{25}Ni_{20}$ was mounted in transmission geometry. In this alloy the ^{57}Fe nuclei exhibit a single-line resonance. While the foil was moved back and forth in a constant-acceleration mode [i.e., with a linear variation of the Doppler shift $E_D = (v_D/c)E_0$], delayed resonant quanta within a time interval (t_1, t_2) were counted as function of E_D (*23*). Figure 3 shows the measured energy spectra of both samples being aligned to their first-order guided modes. In both cases, the center of mass of the measured spectra was shifted toward negative energies with values of $-5.1\Gamma_0$ for sample 1 and $-9.0\Gamma_0$ for sample 2. These values are reproduced by Eq. 4 within a margin of about ±5%, which confirms that the collective Lamb shift in this approximation is proportional to the extension (thickness) of the nuclear ensemble. The solid lines in Fig. 3 are theoretical simulations (*23*), indicating a good agreement with the measured spectra. The asymmetric shape of the energy spectra is a consequence of the residual quadrupole hyperfine interaction to which the ^{57}Fe nuclei are subjected (*29*). For comparison, the dashed lines in Fig. 3 are calculations with vanishing quadrupole interaction, indicating that the measurement of the radiative level shift is not affected by the hyperfine interaction (except for an isomer shift) of the nuclei in the sample.

Under grazing angles, the relevant component of the wave vector is the one normal to the surface, $k_{0z} \approx \varphi k_0$, and therefore $k_{0z}R << 1$. Thus, all nuclei within the thin layer experience the same amplitude and phase in the standing wave pattern of the cavity mode while being confined to a dimension that is small relative to the field wavelength $\lambda_z = 2\pi/k_{0z}$. As a result, the relative phases in Eq. 1 are equal modulo 2π, so that effectively the small-sample limit $k_0R << 1$ of Dicke superradiance is realized. In this limit the sample effectively appears to be two-dimensional, where the collective Lamb shift scales with the areal density ρ_A of the nuclei as $L_N \sim \rho_A\lambda^2$. This is in contrast to three-dimensional samples such as a spherical cloud, for which the collective Lamb shift scales as $L_N \sim \rho\lambda^3$ (*3*, *5*). Because ρ_A can be easily adjusted via the layer thickness, the planar cavity appears to be an attractive system for studying cooperative optical phenomena.

References and Notes

1. W. E. Lamb Jr., R. C. Retherford, *Phys. Rev.* **72**, 241 (1947).
2. H. A. Bethe, *Phys. Rev.* **72**, 339 (1947).
3. R. Friedberg, S. R. Hartmann, J. T. Manassah, *Phys. Rep. C* **7**, 101 (1973).
4. A. Svidzinsky, J. T. Chang, *Phys. Rev. A* **77**, 043833 (2008).
5. M. O. Scully, *Phys. Rev. Lett.* **102**, 143601 (2009).
6. M. O. Scully, A. A. Svidzinsky, *Science* **325**, 1510 (2009).
7. R. Friedberg, J. T. Manassah, *Phys. Lett. A* **373**, 3423 (2009).
8. J. T. Manassah, *Laser Phys.* **20**, 259 (2010).
9. R. Friedberg, J. T. Manassah, *Phys. Lett. A* **374**, 1648 (2010).
10. W. R. Garrett, R. C. Hart, J. E. Wray, I. Datskou, M. G. Payne, *Phys. Rev. Lett.* **64**, 1717 (1990).
11. R. Friedberg, S. R. Hartmann, J. T. Manassah, *Phys. Rev. A* **39**, 93 (1989).
12. R. H. Dicke, *Phys. Rev.* **93**, 99 (1954).
13. N. Skribanowitz, I. P. Herman, J. C. Mac Gillivray, M. S. Feld, *Phys. Rev. Lett.* **30**, 309 (1973).
14. M. Gross, S. Haroche, *Phys. Rep.* **93**, 301 (1982).
15. M. O. Scully, E. S. Fry, C. H. R. Ooi, K. Wódkiewicz, *Phys. Rev. Lett.* **96**, 010501 (2006).
16. J. P. Hannon, G. T. Trammell, *Hyperfine Interact.* **123–124**, 127 (1999).
17. M. O. Scully, *Laser Phys.* **17**, 635 (2007).
18. I. E. Mazets, G. Kurizki, *J. Phys. B* **40**, F105 (2007).
19. U. van Bürck, *Hyperfine Interact.* **123–124**, 483 (1999).
20. B. W. Adams, *J. Mod. Opt.* **56**, 1974 (2009).
21. D. J. Heinzen, M. S. Feld, *Phys. Rev. Lett.* **59**, 2623 (1987).
22. $c_N = \{f_{LM}/[2(1 + \alpha)]\}[(2I_e + 1)/(2I_g + 1)]$, where f_{LM} is the Lamb-Mössbauer factor, α is the coefficient of internal conversion, and I_g and I_e are the nuclear spins of the ground and excited state, respectively. For metallic ^{57}Fe at room temperature, $f_{LM} \approx 0.8$, so that $c_N \approx 0.09$.
23. See supporting material on *Science* Online.
24. W. Sturhahn, E. Gerdau, *Phys. Rev. B* **49**, 9285 (1994).
25. R. Röhlsberger, *Hyperfine Interact.* **123–124**, 301 (1999).
26. W. Sturhahn, *Hyperfine Interact.* **125**, 149 (2000).
27. C. Leonardi, A. Vaglica, *Nuovo Cim. B* **67**, 256 (1982).
28. V. V. Temnov, U. Woggon, *Phys. Rev. Lett.* **95**, 243602 (2005).
29. Because the energetic width of the cavity resonance (~100 eV) is much larger than the width of the nuclear response (~300 neV), any impact of the cavity resonance on the nuclear spectral shape can be excluded (weak-coupling limit of cavity QED).

30. We thank A. N. Poddubny for valuable discussions and for helpful comments on the manuscript; H. Lipkin, J. T. Manassah, B. W. Adams, and K. Temst for fruitful discussions on this and related topics; and W. Pfützner for assistance during sample preparation. Supported by the Geconcerteerde Onderzoeksacties and Fonds Wetenschappelijk Onderzoek Flanders programs (S.C.).

Supporting Online Material

www.sciencemag.org/cgi/content/full/science.1187770/DC1
Materials and Methods
Figs. S1 to S3
References

1 February 2010; accepted 13 April 2010
Published online 13 May 2010;
10.1126/science.1187770
Include this information when citing this paper.

Dynamic Kinetic Resolution of Biaryl Atropisomers via Peptide-Catalyzed Asymmetric Bromination

Jeffrey L. Gustafson, Daniel Lim, Scott J. Miller*

Despite the widespread use of axially chiral, or atropisomeric, biaryl ligands in modern synthesis and the occurrence of numerous natural products exhibiting axial chirality, few catalytic methods have emerged for the direct asymmetric preparation of this compound class. Here, we present a tripeptide-derived small-molecule catalyst for the dynamic kinetic resolution of racemic biaryl substrates. The reaction proceeds via an atropisomer-selective electrophilic aromatic substitution reaction using simple bromination reagents. The result is an enantioselective synthesis that delivers chiral nonracemic biaryl compounds with excellent optical purity and good isolated chemical yields (in most cases a >95:5 enantiomer ratio and isolated yields of 65 to 87%). A mechanistic model is advanced that accounts for the basis of selectivity observed.

The stereochemical implications of hindered rotation in nonplanar molecules, termed atropisomerism, have intrigued chemists for at least 89 years (*1*, *2*). Atropisomeric compounds exhibit an axis of chirality (Fig. 1A), rather than a stereogenic atom, such as an sp^3-hybridized carbon with four distinct substituents (Fig. 1B). The capacity of the single bond between two aromatic rings to freely rotate is the basis of racemization for many atropisomeric compounds (*3*). Yet in naturally occurring compounds, atropisomeric molecules are often found in single isomeric form because of substituents on aryl rings that raise the barriers to racemization. Also, the localization of aryl rings within multicyclic ring systems can constrain single bond rotations, preventing isomerization and the observation of mixtures (*4*, *5*). These properties no doubt contribute to the remarkable structures and functions of numerous biologically active compounds that contain single atropisomers as part of their structure (*6*). Perhaps the glycopeptide antibiotic vancomycin is the signature bioactive natural product of this type (Fig. 1C). The chiral ligand BINAP [2,2′-bis(diphenylphosphino)-1,1′-binaphthyl] (Fig. 1D), a venerable ligand for

Department of Chemistry, Yale University, 225 Prospect Street, Post Office Box 208107, New Haven, CT 06520–8107, USA.

*To whom correspondence should be addressed. E-mail: scott.miller@yale.edu